

ARTICLE

Received 7 May 2014 | Accepted 25 Jun 2014 | Published 24 Jul 2014

DOI: 10.1038/ncomms5514

PINK1 deficiency sustains cell proliferation by reprogramming glucose metabolism through HIF1

Raquel Requejo-Aguilar^{1,2}, Irene Lopez-Fabuel^{1,2}, Emilio Fernandez^{1,2}, Luis M. Martins³, Angeles Almeida^{1,2} & Juan P. Bolaños^{1,2}

PTEN-induced kinase-1 (PINK1) is a Ser/Thr kinase implicated in familial early-onset Parkinson's disease, and was first reported as a growth suppressor. PINK1 loss-of-function compromises both mitochondrial autophagy and oxidative phosphorylation. Here we report that PINK1 deficiency triggers hypoxia-inducible factor-1 α (HIF1 α) stabilization in cultured *Pink1*^{-/-} mouse embryonic fibroblasts and primary cortical neurons as well as *in vivo*. This effect, mediated by mitochondrial reactive oxygen species, led to the upregulation of the HIF1 target, pyruvate dehydrogenase kinase-1, which inhibits PDH activity. Furthermore, we show that HIF1 α stimulates glycolysis in the absence of *Pink1*, and that the promotion of intracellular glucose metabolism by HIF1 α stabilization is required for cell proliferation in *Pink1*^{-/-} mice. We propose that loss of *Pink1* reprograms glucose metabolism through HIF1 α , sustaining increased cell proliferation.

¹Institute of Functional Biology and Genomics (IBFG), University of Salamanca-CSIC, 37007 Salamanca, Spain. ²Institute of Biomedical Research of Salamanca (IBSAL), University Hospital of Salamanca, 37007 Salamanca, Spain. ³MRC Toxicology Unit, Hodgkin Building, Leicester LE1 9HN, UK. Correspondence and requests for materials should be addressed to J.P.B. (email: jbolanos@usal.es).

Parkinson's disease (PD) is the second most common neurodegenerative disease, affecting 1–2% of people over 65 years of age. PD is characterized by the loss of dopaminergic neurons and the development of intracellular aggregates of the protein α -synuclein. Currently, it is widely accepted that mitochondrial dysfunction is a key factor in PD pathogenesis¹. While the vast majority of PD cases are sporadic, 5–10% of cases are inherited through mutations in PD-related genes. There is now compelling evidence supporting the notion that the autosomal recessive early-onset PD-related genes PTEN-induced kinase-1 (*PINK1*) and *PARKIN* are key regulators of the mitochondrial quality control^{2,3}.

Full-length *PINK1* localizes to the mitochondrial outer membrane^{3,4}, where it interacts—in a phosphorylation-dependent manner—with *PARKIN*^{5,6}, both acting on the same pathway as a quality control system to preserve mitochondrial integrity on mitochondrial membrane potential ($\Delta\psi_m$) collapse. Thus, loss of *PINK1*, or disease-relevant mutations in *PINK1* gene, compromises mitochondrial autophagy^{7–10}, as well as mitochondrial oxidative phosphorylation, predominantly at the level of complex I^{11,12}.

Besides its role in PD, *PINK1* was reported to have a growth suppressive function¹³ through a yet unravelled mechanism. Given that cell proliferation requires, among other metabolic adaptations, a high glycolytic rate¹⁴ and, in view of its mitochondrial protection role, we hypothesized that *PINK1* might act by modulating glycolysis. Here, we show that the loss of *Pink1* reprograms glucose metabolism through hypoxia-inducible factor-1 α (HIF1 α) to stimulate glycolysis. Unexpectedly, we found that the glycolytic reprogramming is required for the increased cell proliferation observed on loss of *Pink1*.

Results

Loss of *Pink1* stimulates glucose metabolism. To elucidate whether *PINK1* regulates glucose metabolism, we first obtained *Pink1*^{−/−} (*Pink1* knockout or KO) and *Pink1*^{+/+} (wild type or WT) primary mouse embryonic fibroblasts (MEF) from the same offspring. The rates of glucose uptake (Fig. 1a) and glycolysis (Fig. 1b,c) in *Pink1* KO MEF were approximately twofold higher when compared with WT. Instead, the rate of glucose utilization through the pentose–phosphate pathway (PPP) was ~45% lower in *Pink1* KO MEF than in WT (Fig. 1d), indicating the shift of glucose-6-phosphate consumption from PPP towards glycolysis that also takes place in other biological settings¹⁵. To extend these findings to non-proliferating cells, we next assessed glucose metabolism in cultured primary cortical neurons. As shown in Fig. 1e–g, loss of *Pink1* in neurons triggered a ~twofold increase in the rates of glucose uptake and glycolysis when compared with WT. The flux of glucose consumption through the PPP was reduced in a similar extent in *Pink1* KO neurons (Fig. 1h), suggesting metabolic shift from PPP to glycolysis in neurons. We next sought to confirm the enhanced glucose metabolism *in vivo*. We found that *Pink1* KO mice were slightly hypoglycaemic (Fig. 1i) and hyperlactatemic (Fig. 1j). In addition, the rate of ¹⁴C-lactate appearance in the blood from acutely injected [U-¹⁴C]glucose mice was higher in *Pink1* KO than in WT (Fig. 1k). Together, these results indicate that the loss of *Pink1* causes a metabolic reprogramming that promotes glucose uptake and glycolysis.

Glucose-utilizing enzymes and HIF1 α are altered on loss of *Pink1*. To investigate whether the changes in glucose metabolism

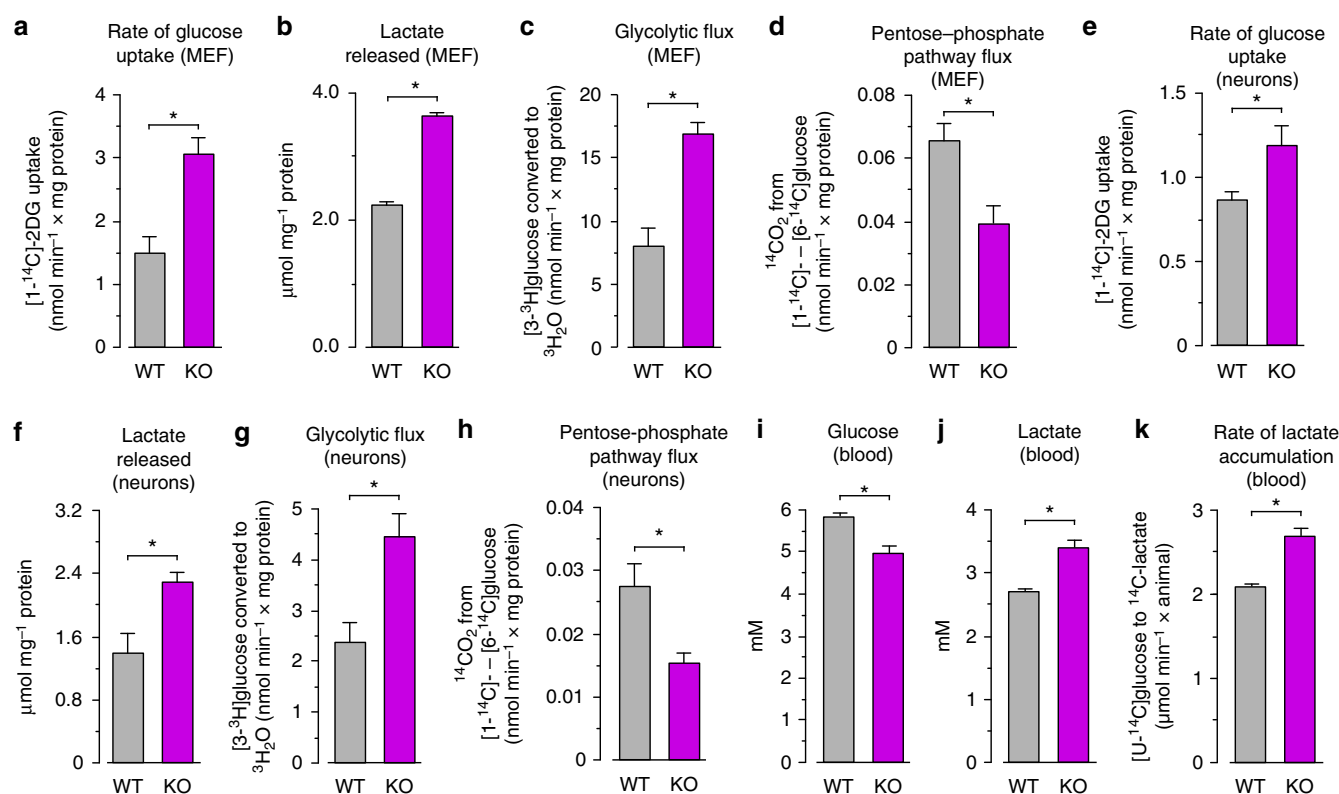


Figure 1 | Enhanced glucose metabolism on loss of *Pink1*. The rate of glucose uptake (a,e), lactate released after 4 h of incubation (b,f), glycolytic flux (c,g) and pentose–phosphate flux (d,h) were assessed in MEF and mouse cortical neurons in primary culture, as indicated, obtained from either WT or *Pink1* KO (*Pink1*^{−/−}) mice. Blood concentrations of glucose (i) and lactate (j), and the rate of ¹⁴C-lactate appearance in the blood from acutely injected [U-¹⁴C]glucose in the tail vein (k) of WT and *Pink1* KO mice were analysed. Data are expressed as mean \pm s.e.m. **P* < 0.05 (Student's *t*-test; *n* = 3–4 independent experiments).

observed by the loss of *Pink1* were associated with alterations in the expression of glycolytic enzymes, we next analysed the relative messenger RNA (mRNA) abundance of key glucose-metabolizing enzymes. As shown in Fig. 2a, glucose transporter-1 (*Glut1*), glucose transporter-3 (*Glut3*), hexokinase-2 (*Hk2*) and glyceraldehyde-3-phosphate dehydrogenase (*Gapdh*) mRNA abundances, relative to those of the housekeeping β -Actin, were ~ 1.5 – 2.5 -fold higher in *Pink1* KO MEF when compared with WT. The relative mRNA abundance of other key glycolytic enzymes, including 6-phosphofructo-2-kinase/fructose-2,6-bisphosphatase-3, enolase-1 and lactate dehydrogenase-a, but not that of hexokinase-1, albeit very slightly, were also higher in the *Pink1* KO MEF than in WT (Supplementary Fig. 1a). The protein levels of GLUT1, HK2 and GAPDH were also increased in the *Pink1* KO MEF (Fig. 2b; Supplementary Fig. 1b); GLUT3 protein was undetectable in MEF (not shown). As these transporters and enzymes are well-known targets of hypoxia-inducible factor-1 (HIF1), we next investigated the abundance of its α -subunit (HIF1 α) that is amenable to regulation by protein stability¹⁶. As shown in Fig. 2b, HIF1 α protein was increased in MEF lacking *Pink1* (see, also, Supplementary Fig. 1b). Since this effect cannot be ascribed to a putative increase in *Hif1 α* mRNA abundance (*Hif1 α* levels in *Pink1* KO MEF were found to be 0.49 plus or minus (\pm) 0.07-fold, normalized to β -actin, when compared with WT; $n = 3$), our data indicate the stabilization of HIF1 α in the *Pink1* KO MEF. Likewise, cultured primary neurons from the *Pink1* KO mice had ~ 1.4 – 1.8 -fold enhancement in the mRNA abundances of *Glut1*, *Glut3*, *Hk2* and *Gapdh* when compared with WT (Fig. 2c). The corresponding proteins were increased accordingly (Fig. 2d; Supplementary Fig. 1c). In *Pink1* KO neurons, HIF1 α protein—but not its mRNA (*Hif1 α* levels in *Pink1* KO neurons were found to be 0.43 ± 0.11 -fold, normalized to β -actin, when compared with WT; $n = 3$)—was higher than in WT (Fig. 2d; Supplementary Fig. 1c). To extend our observations to *in vivo* settings, we confirmed the upregulation of GLUT1, GLUT3 and HIF1 α in skeletal muscle of *Pink1* KO mice (Figs 1d, 2e). In addition, we performed a microRNA (miR) transcription profiling in *Pink1* KO mice brain, which revealed significantly elevated several miRs, such as *miR-30b-5p*,

miR-26b-5p, *miR-27a-3p*, *miR-181c-5p*, *miR-494-3p* and *miR-30d-5p* that are reported to modulate HIF1 α repression¹⁷ (Supplementary Table 1). Thus, our data indicate HIF1 α stabilization in the *Pink1*-null mice, and HIF1 α -target proteins enhancement likely contributing to the observed glucose metabolism reprogramming.

HIF1 α is required for increased glycolysis on *Pink1* loss. To directly demonstrate the involvement of HIF1 α in the glycolytic phenotype caused by loss of *Pink1*, we explored the consequences of its removal by RNA interference. As shown in Fig. 3a, transfection of MEF with a small interfering RNA (siRNA) against *Hif1 α* (*siHif1 α*) showed an $\sim 60\%$ decrease in *Hif1 α* mRNA abundance when compared with controls. This effect was selective since *siHif1 α* was unable to knockdown the HIF1 α protein that was expressed from a mutant form of *Hif1 α* cDNA harbouring silent mutations on its siRNA-target region (Fig. 3b; Supplementary Fig. 2a). HIF1 α knockdown fully prevented the increase in the *Glut1*, *Glut3*, *Hk2* and *Gapdh* mRNA abundance (Fig. 3c), and in the GLUT1 and GAPDH (Fig. 3d; Supplementary Fig. 2b) protein abundance of the *Pink1* KO MEF. Furthermore, the increased lactate released (Fig. 3e) and glycolytic rate (Fig. 3f) promoted by PINK1 loss-of-function was rescued by knocking down HIF1 α . Likewise, knocking down HIF1 α in primary neurons (Fig. 3g; Supplementary Fig. 2c) fully abolished the increase in the glycolytic rate exerted by PINK1 loss-of-function (Fig. 3h). Together, these data strongly suggest that HIF1 α is required for the enhanced glycolytic phenotype caused by the loss of *Pink1*.

Mitochondrial ROS mediate HIF1 α stabilization on *Pink1* loss.

To understand how the lack of PINK1 upregulated HIF1 α , we first confirmed the defects in both mitochondrial respiratory chain (Fig. 4a) and inner membrane potential (Fig. 4b) of *Pink1* KO MEF that were previously reported in similar settings^{11,18}. Moreover, we found that pyruvate dehydrogenase kinase-1 (PDK1) protein abundance, a known HIF1-target¹⁹, was higher in *Pink1* KO MEF when compared with WT (Fig. 4c; Supplementary Fig. 2e). In addition, we found that the increase

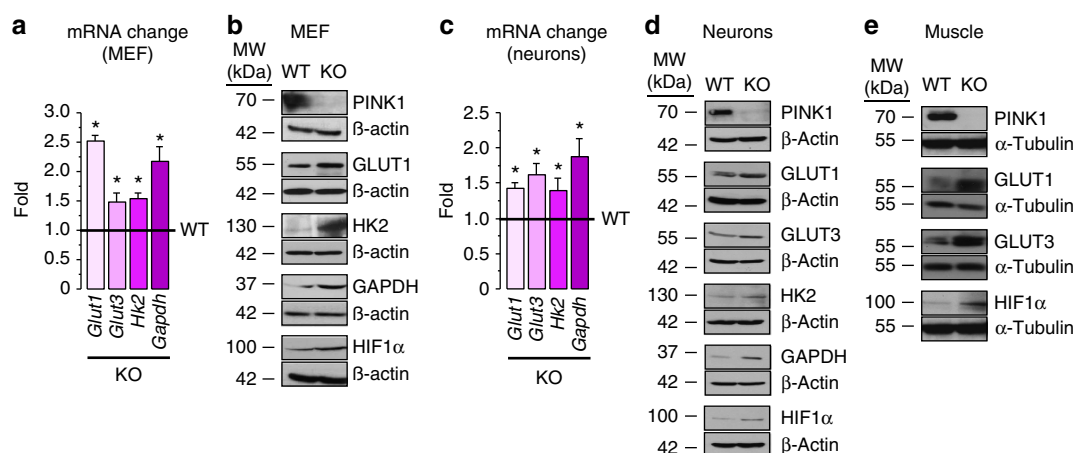


Figure 2 | Glucose-utilizing enzymes and HIF1 α are altered by *Pink1* loss. Quantitative real-time PCR (RT-qPCR) analysis of the relative mRNA abundances of *Glut1*, *Glut3*, *Hk2* and *Gapdh* in WT and *Pink1* KO mice MEF (a) or neurons (c). β -Actin mRNA was used for normalization, and the *Pink1* KO data are expressed as the change relative to WT. Western blot analysis of the protein abundances of PINK1, GLUT1, GLUT3 (not detectable in MEF), HK2, GAPDH and HIF1 α in WT and *Pink1*-null mice MEF (b) or neurons (d); β -Actin was used as loading control. (e) Western blot against PINK1, GLUT1, GLUT3 and HIF1 α in WT and *Pink1* KO mice skeletal muscle samples; α -Tubulin was used as loading control. Only representative western blots are shown per condition; the replicates and the semi-quantitative estimation of the band intensities are shown in the Supplementary Information. The mean \pm s.e.m. values of the mRNA data were calculated from the fold change of each β -Actin-normalized transcript abundance in the *Pink1* KO samples versus that in the WT. Thus, in all cases, the WT values were considered = 1.00. * $P < 0.05$ versus the corresponding WT (Student's *t*-test; $n = 3$ –4 independent experiments).

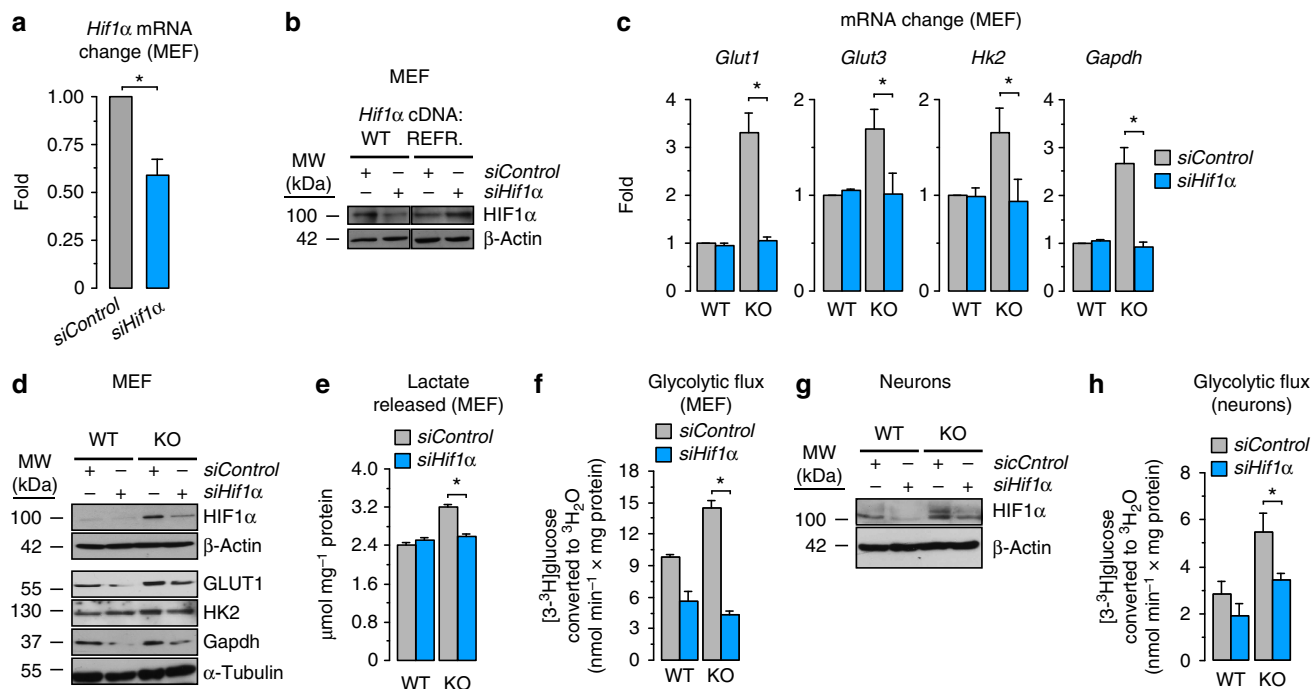
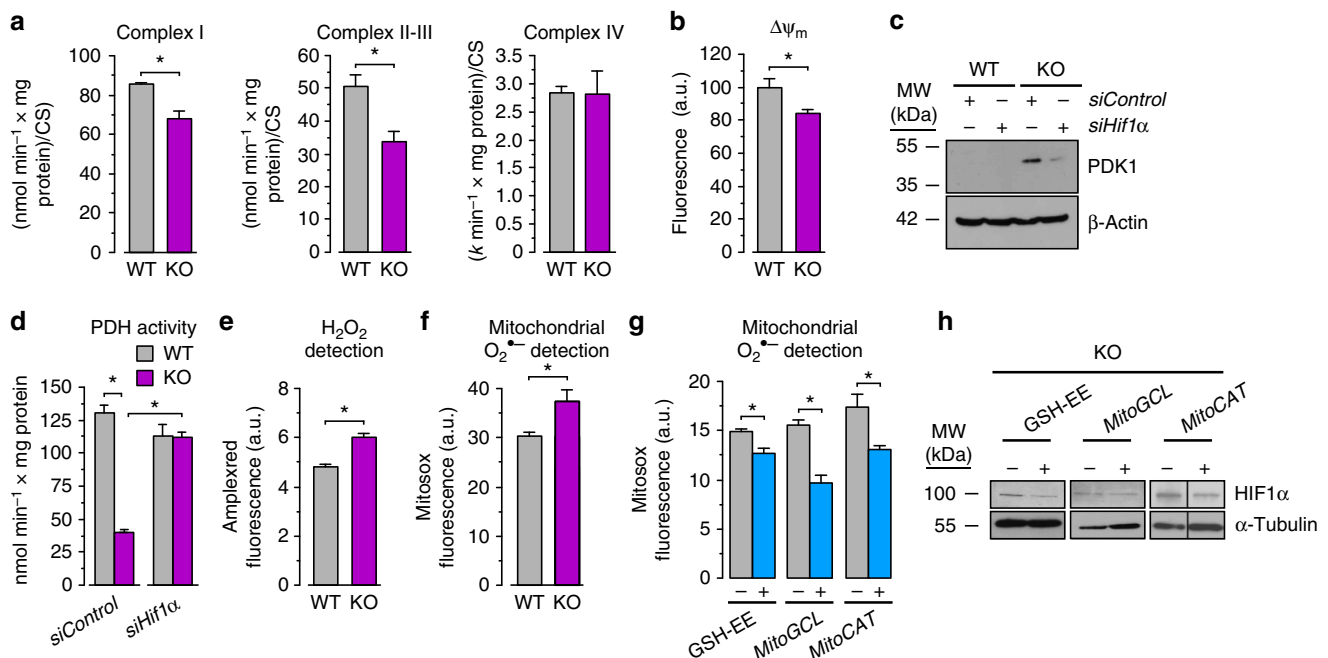


Figure 3 | HIF1α is required for increased glycolysis by *Pink1* loss. An *siHif1α* was used to evaluate its involvement in the glycolytic phenotype of *Pink1* KO cells. **(a)** RT-qPCR analysis of *Hif1α* mRNA abundance in MEF transfected with *siHif1α*, or *siControl* (100 nM), after 72 h. **(b)** *siHif1α* effectively knockdowns expressed *Hif1α* cDNA WT, but not a *Hif1α* cDNA silent mutant form refractory to *siHif1α* (*Hif1α* cDNA REFR.) in mice MEF. **(c)** RT-qPCR analysis of the relative mRNA abundances of *Glut1*, *Glut3*, *Hk2* and *Gapdh* in WT and *Pink1* KO mice MEF transfected with *siControl* or *siHif1α*. *β-Actin* mRNA was used for normalization, and all data are expressed as the change relative to WT-*siControl*. **(d)** Western blot against HIF1α in WT and in *Pink1* KO mice MEF transfected with *siHif1α* or *siControl* shows the efficacy of the *siHif1α* at knocking down endogenous HIF1α; *β-actin* was used as loading control. As shown, *siHif1α* partially prevented the increase in GLUT1, HK2 and GAPDH protein abundances. The increased rate of lactate released after 4 h of incubation **(e)** and glycolytic flux **(f)** observed in the *Pink1* KO MEF was prevented by *siHif1α*. *siHif1α* was also effective at preventing the endogenous increased HIF1α protein **(g)**, as well as the increased glycolytic flux **(h)** observed in *Pink1* KO primary neurons. Only representative western blots are shown; the replicates and the semi-quantitative estimation of the band intensities are shown in the Supplementary Information. The mean ± s.e.m. values of the mRNA data were calculated from the fold change of each *β-actin*-normalized transcript abundance in the *Pink1* KO samples versus that in the WT **(a)** or WT-*siControl* **(c)**; thus, in all these cases, the WT **(a)** or WT-*siControl* **(c)** values were considered = 1.00. Only the statistical analysis results of the *siHif1α* versus *siControl* (in KO) values (mean ± s.e.m.) are shown in **c,e,f,h**, since the comparison KO versus WT under control conditions was previously shown in Fig. 2a, Fig. 1b,c,g, respectively. **P* < 0.05 (Student's *t*-test; *n* = 3–4 independent experiments).

in PDK1 protein was abolished by knocking down HIF1α (Fig. 4c; Supplementary Fig. 2e). Since PDK1 phosphorylates PDH, complex inhibiting its activity, we next determined PDH activity in the *Pink1* KO MEF. As shown in Fig. 4d, PDH activity was ~80% lower in *Pink1* KO cells when compared with WT, and this effect was ablated by HIF1α knockdown. Thus, through HIF1, PINK1 deficiency inhibits PDH activity, which likely contributes to a positive loop of mitochondrial impairment. Confirming previous work¹⁸, we found that the rates of H₂O₂ and mitochondrial O₂^{•-} detected were higher in MEF from *Pink1* KO mice than in the WT (Fig. 4e,f). Since these reactive oxygen species (ROS) stabilize HIF1α^{20–22}, we sought to assess whether mitochondrial ROS mediated the enhancement of HIF1α observed by the loss of PINK1. As shown in Fig. 4g, mitochondrial O₂^{•-} detection was reduced either by incubating MEF with a plasma membrane permeable form of glutathione (glutathione ethyl ester, GSH-EE), or by expressing mitochondrial-tagged forms of glutamate-cysteine ligase (*mitoGCL*)²³ or catalase (*mitoCAT*). As depicted in Fig. 4h and Supplementary Fig. 2f, the increase in HIF1α protein observed in *Pink1* KO MEF was decreased not only by the whole-cell ROS scavenger GSH-EE, but also by selectively removing ROS in mitochondria with *mitoGCL* or *mitoCAT*. Thus, mitochondrial-derived ROS accounts for HIF1α protein stabilization caused by *Pink1* loss.

Increased cell proliferation on loss of *Pink1* requires HIF1α.

Given that PINK1 is a growth-suppressor protein¹³ and that increased glucose utilization supports cell growth¹⁴ through HIF1 (ref. 16), we next sought to determine whether the observed increased rate of glycolysis in *Pink1* KO cells was associated with an increase in cell proliferation. To achieve this, we evaluated the rate of bromo-deoxy-uridine (BrdU) incorporation into DNA, the proportion of each cell cycle phase, and cell growth in *Pink1* KO MEF in the absence or in the presence of the glucose-metabolizing inhibitor, 2-deoxyglucose (2DG). As depicted in Fig. 5a, *Pink1* KO MEF showed a higher rate of BrdU incorporation, decreased G₀/G₁ phase, increased S and G₂/M phases and higher rate of proliferation (Fig. 5b) when compared with WT; moreover, 2DG fully abolished *Pink1* KO-mediated increase in cell proliferation (Fig. 5a,b), indicating the requirement of glucose utilization for *Pink1* KO-induced cell proliferation. In addition, the increased proliferation rate of the *Pink1* KO MEF was prevented by knocking down HIF1α (Fig. 5c,d), indicating the requirement of HIF1α stabilization for *Pink1* KO-induced cell proliferation. To confirm the high proliferative status *in vivo*, we analysed the neurogenic subventricular zone (SVZ) in the *Pink1* KO mouse brain. As shown in Fig. 5e, we observed a ~twofold increase in Ki67-immunostained cells that were positive for the stem cell marker Sox2, confirming enhanced proliferation rate of neural



stem cells *in vivo* by *Pink1* loss. Thus, our data shows that the loss of PINK1 causes an increase in cell proliferation, for which both glucose utilization and HIF1 α are required. Primary neurons, obtained from the *Pink1* KO mice, showed higher mitochondrial-derived ROS than WT (Fig. 6a), likely contributing—such as in MEF—to HIF1 α stabilization. However, in line with their post-mitotic status, these *Pink1* KO neurons showed unaltered their rate of BrdU incorporation rate (Fig. 6b); we found, instead an increased apoptotic cell death rate (Fig. 6c). Thus, the metabolic re-wiring caused by PINK1 loss-of-function, being unable to support proliferation in post-mitotic neurons, would likely be involved in a death phenotype.

Discussion

Here, we show that loss of *Pink1* reprograms glucose metabolism and this is likely to meet the bioenergetic requirements for the enhanced proliferation observed in *Pink1* knockout proliferating cells such as fibroblasts. Moreover, we have also identified ROS-mediated HIF1 α stabilization as the molecular mechanism responsible for this metabolic adaptation. According to our results obtained with mitochondrial-tagged antioxidant enzymes, mitochondrial-derived ROS are likely to play a key role in HIF1 α stabilization. However, the involvement of cytosolic ROS in this effect cannot be discarded. In fact, decreased catalase and peroxiredoxin have been linked to the loss of PINK1 in other vertebrates such as zebrafish¹⁸. This may also account for the ROS increase observed by us in *Pink1*-null cells. In addition, a decrease in *Hif1 α* mRNA has been

previously reported in the *Pink1* KO zebrafish²⁴, and in *Pink1* KO MEF and neurons on hypoxia²⁵. Here, we detected higher HIF1 α protein levels in spite of a lower *Hif1 α* mRNA abundance under normoxia that could represent a compensatory response to HIF1 α stabilization.

The upregulation of glucose metabolism on *Pink1* loss reported here apparently contrasts with a previous study reporting impaired glucose uptake in *Pink1* KO neurons^{18,26}. While reasons for this discrepancy are unclear, it should be noted that we found both increased glucose uptake and glycolysis rates at ~5 mM glucose concentration, instead at the very low (0–2 mM) glucose concentrations previously used^{18,26}. Furthermore, we confirmed the increased glucose consumption using *in vivo* settings, as well as the requirement for HIF1 α -enhanced glycolysis to maintain the high proliferative status of *Pink1*-null cells. We were surprised that the molecular mechanism identified in this study results in a proliferative phenotype in dividing *Pink1* KO cells. Interestingly, PD patients harbouring mutant PINK1 were reported to have increased astroglial proliferation²⁷, which could be accounted for by the metabolic alterations described here. In line with this observation, it has been shown that the loss of function of the downstream PINK1 target, PARKIN^{5,6}—as well as the loss of function of other PD-linked genes—is associated with increased cancer prevalence²⁸. Therefore, it seems likely that PINK1 regulates cell proliferation through PARKIN. In addition, our data, showing enhanced proliferating activity of neural stem cells in the *Pink1*-null mice brains, suggests a potentially unexpected key regulatory role for PINK1 in the metabolic adaptation of stem cells.

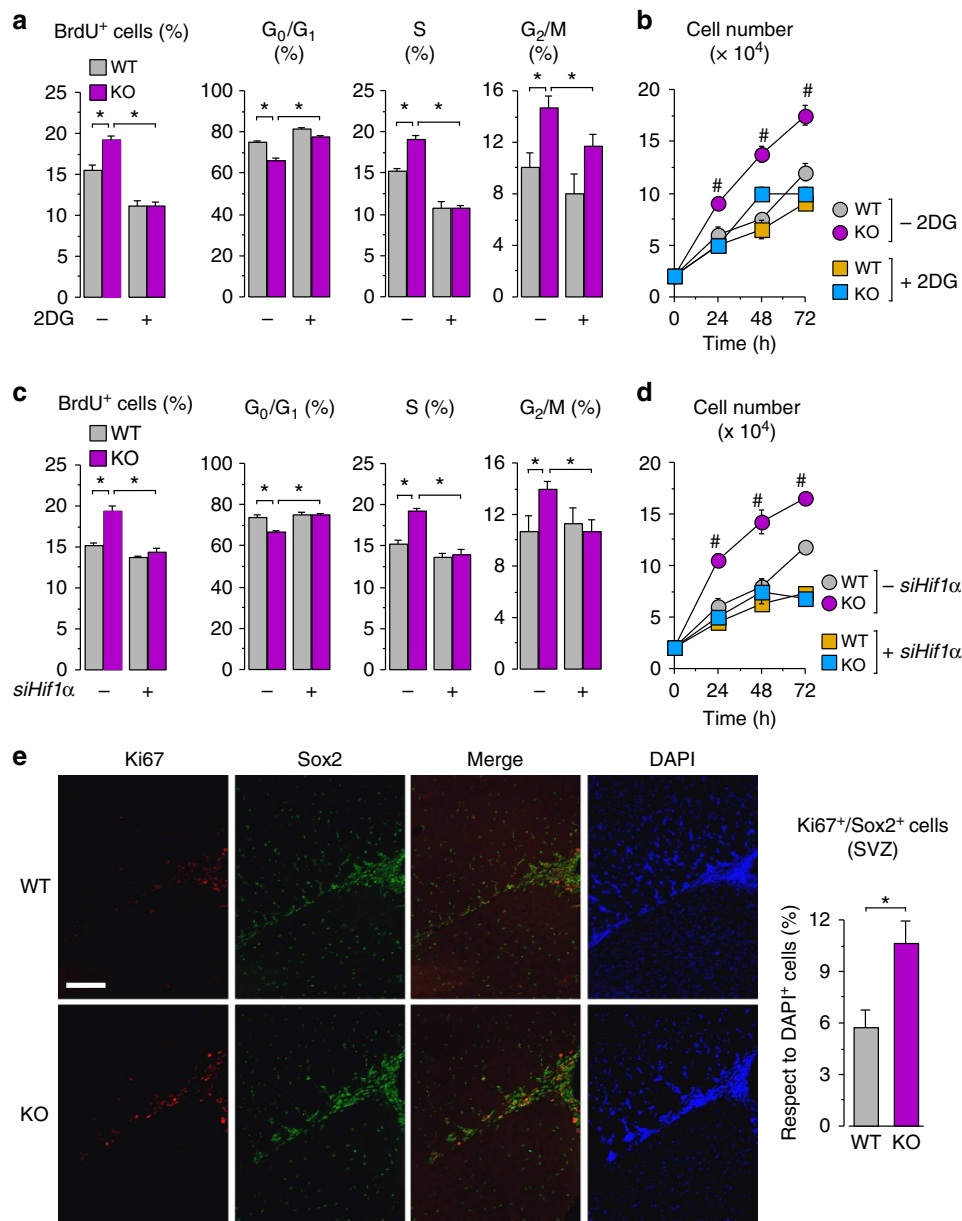


Figure 5 | Increased cell proliferation by *Pink1* loss requires *HIF1α*. (a) Proportion of BrdU incorporation into DNA and cell cycle phases, and (b) cell growth in WT and *Pink1* KO MEF after 72 h in the absence (denoted as -2DG) or in the presence (+2DG) of the glucose-metabolizing inhibitor, 2-deoxyglucose (2DG, 1 mM). (c) Proportions of BrdU incorporation into DNA and cell cycle phases, and (d) cell growth in WT and *Pink1* KO MEF 72 h after transfection with *siHif1α* (+*siHif1α*) or *siControl* (denoted as -*siHif1α*). (e) Ki67, Sox2 and DAPI immunostaining in the subventricular zone of WT and *Pink1* KO mouse brain, and the corresponding quantification. * $P < 0.05$; # $P < 0.05$ versus all other conditions (analysis of variance followed by Bonferroni test; $n = 3-4$ independent experiments). All data are expressed as mean \pm s.e.m. Scale bar, 100 μ m.

Whether PD-relevant loss-of-function mutations on the *PINK1* gene confer the high glycolytic phenotype that we describe here deserves further investigation; however, this is likely to be the case since such mutations also lead to mitochondrial oxidative phosphorylation defects¹² that are responsible for the switch from mitochondrial oxidative to glycolytic metabolism¹⁶. Some *PINK1* single nucleotide polymorphic genotypes are associated with type 2 diabetes and obesity²⁹, thus further studies focusing on glucose homeostasis and PD may be worth pursuing. Besides contributing to the observed enhanced proliferative rates detected in *Pink1*-null fibroblasts, the metabolic reprogramming observed on loss of *Pink1* could also sustain mitochondrial proliferation in non-dividing cells such as neurons. In line with this concept, *pink1* mutant flies activate a signalling pathway that attempts to

compensate for mitochondrial dysfunction by inducing mitochondrial proliferation in post-mitotic cells³⁰. The metabolic re-wiring identified in our study may also contribute to cellular damage on *PINK1* loss. In this context, post-mitotic neurons subjected to increased glycolytic rate show oxidative stress-mediated neurodegeneration as a consequence of a compensative decreased PPP rate¹⁵. Our data showing such a PPP to glycolysis shift in *Pink1*-deficient cells, including neurons, support the notion that such a mechanism likely contributes to the *Pink1* loss-associated neurodegeneration in PD.

Methods

Ethical statement regarding the use of animals. Mice were bred at the Animal Experimentation Unit of the University of Salamanca, and all protocols were

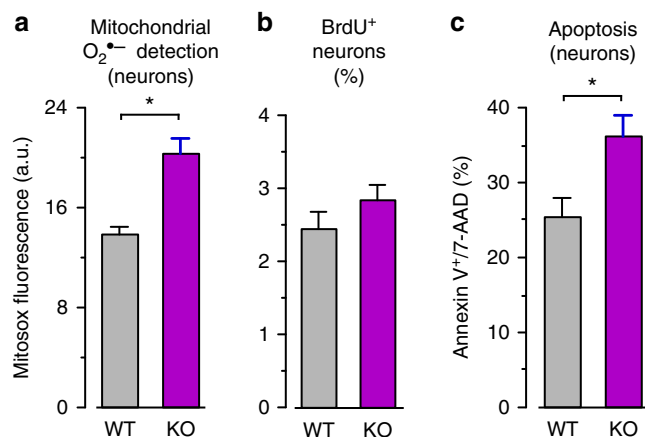


Figure 6 | Loss of Pink1 increases mitochondrial ROS and apoptosis in neurons. (a) Rate of mitochondrial $O_2^{\bullet-}$ detection in WT and *Pink1* KO mice primary neurons. (b) Proportion of BrdU incorporation into DNA of WT and *Pink1* KO neurons. (c) Proportion of apoptosis in WT and *Pink1* KO neurons, as assessed by the proportion of annexin V-positive/7-AAD-negative cells, determined by flow cytometry. Data are expressed as mean \pm s.e.m. * $P < 0.05$ (Student's *t*-test; $n = 3$ –4 independent experiments).

approved by the Bioethics Committee of the University of Salamanca in accordance with the Spanish legislation (RD53/2013). *Pink1* knockout mice were generated by Lexicon Genetics (The Woodlands, Texas, USA); back-crossed for at least nine generations with C57BL/6J WT mice for the experiments and bred under homozygosity.

Cell cultures. MEF were prepared from fetal (E13.5) *Pink1*^{-/-} (*Pink1* KO) and *Pink1*^{+/+} (WT) offspring. Cells were seeded (10^5 cells cm^{-2}) in high glucose (25 mM) DMEM (Sigma, Madrid, Spain) with 10% fetal calf serum (Roche Diagnostics, Heidelberg, Germany) and L-glutamine (4 mM), and incubated at 37 °C in a humidified 5% CO_2 -containing atmosphere. Cortical neurons in primary culture were prepared from fetal (E15.5) WT and *PINK1* KO mice. Cells were seeded at 1.8×10^5 cells cm^{-2} in cell culture plastic dishes previously coated with poly-D-lysine ($15 \mu g ml^{-1}$) in neurobasal medium containing 2% of B-27 supplement (Gibco Brl-Life Technologies, Grand Island, NJ, USA) and 2 mM L-glutamine. Neurons were incubated at 37 °C in a humidified 5% CO_2 -containing atmosphere; at day second, the medium was replaced and neurons were used on the seventh or eighth day *in vitro*.

RNA interference. To knockdown HIF1 α , we used the stealth/siRNA (*siHif1 α*) duplex oligonucleotide 5'-CAAGCAGCAGGAAUUGGAACAUU-3'; as controls (*siControl*), we used the scrambled non-sense siRNA 5'-CAACGAGGAUAAGGUCAUAGCUAU-3' (Invitrogen, Paisley, UK).

Plasmids. To confine the expression of the antioxidant enzymes GCL and catalase to mitochondria, the mitochondrial-tagged full-length cDNA encoding GCL (*mitoGCL*), generated in our laboratory as described²³, and that of catalase (*mitoCAT*), a generous gift from J. A. Enriquez (Centro Nacional de Investigaciones Cardiovasculares, Madrid, Spain), were used. Both *mitoGCL* and *mitoCAT* were subcloned into pIRES2-EGFP (Invitrogen) for transfections. As controls, we used the empty plasmid (pIRES2-EGFP). Full-length cDNA encoding human *Hif1 α* was a generous gift from S. Cadenas (Centro de Biología Molecular Severo Ochoa, Madrid, Spain).

Site-directed mutagenesis. A mutant form of *Hif1 α* cDNA refractory to *siHif1 α* was generated using the site-directed mutagenesis QuikChange XL kit (Stratagene, La Jolla, CA, USA), followed by *DpnI* digestion. The forward and reverse oligonucleotides of the sequence 5'-TCACITTTTCAAGCTGTGGGATCGGGACTTTATTACAGCAGCC-3', carrying silent third-codon base point mutations (mutant nucleotides underlined) was used.

Cell transfections and treatments. Transfection of MEF or neurons with siRNA duplexes were performed using Lipofectamine RNAiMAX reagent (Life Technologies), using 100 nM (final concentration) of the siRNA following the manufacturer's instructions, and cells were used after 3 days. For plasmid transfections, 1.6 μg (per 10^3 cells) of the plasmid was mixed with 1 μM poly-ethylenimine (Sigma) and preincubated for 10 min at room temperature in

Optimem medium (Invitrogen). Cells were then incubated with this poly-ethylenimine/DNA-containing mixture at 37 °C for 1 h, followed by washing with PBS and further incubated in the corresponding culture medium for 24 h. The full-length cDNA encoding human *Hif1 α* , or its *siHif1 α* -refractory mutant form (obtained by site-directed mutagenesis as described above), were also used in co-transfection using Lipofectamine RNAiMAX, each with *siHif1 α* or *siControl* for 24 h. In some experiments, MEF cells were incubated with GSH-E (100 μM for 24 h) or with 2-deoxy-D-glucose (2DG) (1 mM for 72 h).

Assessment of cell proliferation. This was achieved by BrdU incorporation into DNA followed by flow cytometric analysis after a 3-h pulse with BrdU (10 mg ml^{-1}) using the APC BrdU Flow Kit (Becton Dickinson Biosciences, Franklin Lakes, NJ, USA). The proportions of cell cycle phases were also determined by flow cytometric analyses of 7-amino-actinomycin D (7-AAD)-stained cells. Cell proliferation was also confirmed by direct counting under light microscopy.

Real transcriptase quantitative PCR analysis. This was performed in total RNA samples, purified from MEF or neurons using a commercially available kit (Sigma), utilizing the Power SYBR Green RNA-to-CT 1-Step kit (Applied Biosystems, Township, USA). Reverse transcription was performed for 30 min at 48 °C, and PCR conditions were 10 min at 95 °C followed by 40 cycles of 15 s at 95 °C plus 1 min at 60 °C using the primers previously described³¹ (Supplementary Table 2) (purchased from Thermo Scientific, Offenbach, Germany). The mRNA abundance of each transcript was normalized to the β -actin mRNA abundance obtained in the same sample. The resulting normalized values of the *Pink1* knockout samples were expressed as the fold change compared with the corresponding normalized values of the WT samples.

MicroRNA array. RNA was prepared from the cerebral cortex of 6-month-old male mice (eight samples in total, four replicates for each genotype). The RNA quality was confirmed using an Agilent 2100 Bioanalyzer. Detailed experimental protocols and raw data were deposited in ArrayExpress under accession E-MTAB-2462. Differential expression was analysed using R/Bioconductor through standard analysis pipelines.

Western blot. Cells or muscle tissue were lysed in 2% sodium dodecyl sulphate, 2 mM EDTA, 2 mM EGTA, 50 mM Tris, pH 7.5, supplemented with phosphatase inhibitors (1 mM Na_3VO_4 , 50 mM NaF) and protease inhibitors (100 μM phenylmethylsulphonyl fluoride, 50 $\mu g ml^{-1}$ anti-papain, 50 $\mu g ml^{-1}$ pepstatin, 50 $\mu g ml^{-1}$ amastatin, 50 $\mu g ml^{-1}$ leupeptin, 50 $\mu g ml^{-1}$ bestatin and 50 $\mu g ml^{-1}$ soybean trypsin inhibitor), stored on ice for 30 min and boiled for 10 min. Aliquots of the extracts were subjected to sodium dodecyl sulphate polyacrylamide gel electrophoresis (MiniProtein, Bio-Rad, Hercules, CA, USA) and blotted with antibodies overnight at 4 °C. Signal detection was performed with an enhanced chemiluminescence kit (ECL Plus western blotting detection reagent from GE Healthcare, Piscataway Township, NJ, USA). Antibodies used were anti-HIF1 α (1:250; ab16066; Abcam, Cambridge Science Park, Cambridge, UK), anti-PINK1 (1:500; BC100-494; Novus Biologicals, Littleton, CO, USA), anti-HK2 (1:500; sc-6521; Santa Cruz Biotechnology, Dallas, TX, USA), anti- β -actin (1:30,000; A5441; Sigma), α -tubulin (1:2,000; T5168, Sigma), anti-GAPDH (1:40,000; AM4300; Life Technologies, Grand Island, NY, USA), anti-PDK1 (1:1,000; ADI-KAP-PK112; Stressgen-Enzo Life Sciences, Farmingdale, NY, USA), anti-GLUT1 (1:500; 07-1401; EMD Millipore Corporation, Billerica, MA, USA) and anti-GLUT3 (1:250; sc-74497; Santa Cruz Biotechnologies). After incubation with horseradish peroxidase-conjugated goat anti-rabbit IgG (Santa Cruz Biotechnologies), goat anti-mouse IgG (Santa Cruz Biotechnologies), or rabbit anti-goat IgG (Santa Cruz Biotechnologies) (all at 1:10,000 dilution), membranes were immediately incubated with the enhanced chemiluminescence kit SuperSignal West Dura (Pierce, Thermo Scientific, Illinois, USA) for 5 min or Immobilon Western Chemiluminescent HRP Substrate (Merck Millipore; Darmstadt, Germany) for 1 min, before exposure to Kodak XAR-5 film for 1–5 min, and the autoradiograms scanned. Biologically independent replicates (2–5) were always performed; a representative western blot is shown in the main article, and the replicates are shown in the Supplementary Information. The protein abundances were measured by densitometry of the bands on the films using ImageJ 1.48u4 software (National Institutes of Health, USA), and were normalized against the corresponding loading control (β -actin or α -tubulin). The protein abundance was calculated as the ratio of the normalized protein of the *Pink1* KO cells relative to that of the WT, and the resulting values were used for the statistical analysis.

Mitochondrial function parameters and ROS determination. Cells were collected and suspended in 0.1 M potassium phosphate buffer (pH 7.0). After freeze/thawing three times to ensure cellular disruption, NADH-CoQ1 reductase (complex I), succinate-cytochrome *c* reductase (complex II–III), cytochrome *c* oxidase (complex IV) and citrate synthase activities were determined as previously described³². PDH activity was determined in intact mitochondria, isolated as previously described²³ as the rate of [^{14}C]pyruvate decarboxylation to $^{14}CO_2$

(ref. 33). The mitochondrial membrane potential ($\Delta\psi_m$) was assessed using MitoProbe DiI_{C1}(5) Assay Kit for flow cytometry (Molecular Probes Europe BV, Leiden, Netherlands). $\Delta\psi_m$ values were expressed as percentages, using carbonyl cyanide 4-(trifluoromethoxy)phenylhydrazone (FCCP; 10 μ M) to define the 0% $\Delta\psi_m$ values. Mitochondrial superoxide was assessed in intact cells using the fluorescent MitoSox probe (Invitrogen) by flow cytometry, and whole cell-derived H₂O₂ was measured, in intact cells, using the fluorescent AmplexRed probe (Invitrogen), following the manufacturers' instructions.

Rate of glucose uptake. Cultured cells were washed twice with PBS and incubated in a Krebs-Ringer phosphate glucose (KRPB) buffer (145 mM NaCl, 5.7 mM Na₂PO₄, 4.86 mM KCl, 0.54 mM CaCl₂, 1.22 mM MgSO₄ and 5.0 mM glucose, pH 7.4) at 37 °C in the CO₂ incubator. After 1 h, 10 μ l of [1-¹⁴C]-2-deoxyglucose (60 mCi mmol⁻¹; Amersham) was added to the KRPB buffer to a final radioactivity of 0.2 μ Ci ml⁻¹ and cells were incubated for a further 5, 15 and 25 min. At the end of each of these periods of time, the radioactive media was removed and subsequently used to assess the specific radioactivity; cells were rapidly washed three times with ice-cold PBS and immediately lysed with 0.6 ml of 0.1 M NaOH. A 0.5 ml lysate aliquot was used for radioactivity determination using a liquid scintillation counter, and the rest was used to determine protein concentration. The rate of glucose uptake was calculated from the radioactivity versus time regression slopes, which were linear up to the 25 min of incubation. At least four different wells were used for each sample, and at least three different culture preparations were used per condition.

Rates of glycolysis and PPP. These were measured in suspended cells (4–5 × 10⁵ cells), incubated in KRPB buffer in the presence of 5 μ Ci of D-[3-³H]glucose, 0.5 μ Ci ml⁻¹ of D-[1-¹⁴C]glucose or 1 μ Ci ml⁻¹ of [6-¹⁴C]glucose and 5 mM D-glucose in sealed vials. The glycolytic flux was measured by assaying the rate of ³H₂O production from [3-³H]glucose, and the PPP flux as the difference between [1-¹⁴C]glucose and [6-¹⁴C]glucose incorporated into ¹⁴CO₂, as detailed previously¹⁵. *In vivo* blood lactate production was determined 15 min after a tail vein injection of 5 μ Ci of [U-¹⁴C]glucose. Blood [U-¹⁴C]lactate was separated from [U-¹⁴C]glucose by ion exchange chromatography (Dowex AG-1 × 8) as we previously described¹⁵, and measured by liquid scintillation counting. Lactate and glucose concentrations were measured in either cell culture media at the indicated times, or in deproteinized blood samples, by enzymatic analysis spectrophotometrically¹⁵.

Flow cytometric analysis of apoptotic neuronal death. Neurons were carefully detached from the plates using 1 mM EDTA (tetrasodium salt) in PBS. APC-conjugated annexin-V and 7-amino-actinomycin D (7-AAD) (Becton Dickinson Biosciences) were used to determine quantitatively the percentage of apoptotic neurons by flow cytometry. Cells were stained with annexin V-APC and 7-AAD in binding buffer (100 mM HEPES, 140 mM NaCl, 2.5 mM CaCl₂), according to the manufacturer's instructions, and 3 × 10⁵ cells were analysed, in four replicates per condition, on a FACScalibur flow cytometer (15 mW argon ion laser tuned at 488 nm; CellQuest software, Becton Dickinson Biosciences). The annexin V-APC-stained neurons that were 7-AAD-negative were considered to be apoptotic. The analyser threshold was adjusted on the flow cytometer channel to exclude most of the subcellular debris to reduce the background noise owing to the neurite disruption during neuronal detaching. Data were expressed as percentages.

Immunohistochemistry. After deep anaesthesia, mice were perfused intraaortically with 0.9% NaCl, followed by 4% (w/v) paraformaldehyde, 0.2% (w/v) picric acid in 0.1 M phosphate buffer (pH 7.4). Brains were dissected and post fixed overnight and cryoprotected before 20- μ m thick coronal sections were obtained with a freezing-sliding cryostat (Leica CM 1950 AgProtect, Leica, Nussloch, Germany). Sections were incubated with anti-Sox2 antibody (1:4,000; Abcam, ab79351) that stains stem cells, overnight at 4 °C, followed by anti-Ki67 antibody (1:200; Clone SP6; Thermo Scientific), which is expressed in proliferating cells, for 1 h at room temperature. Sections were further incubated with Cy3 anti-rabbit for Sox, and Cy2 anti-mouse for Ki67, followed by DAPI staining. Mounted sections were examined by epifluorescence under a Nikon Inverted microscope (Eclipse Ti-E, Japan) equipped with a precentered fibre illuminator (Nikon Intensilight C-HGFI, Tokyo, Japan) and B/W CCD digital camera (Hamamatsu ORCA-ER, Hamamatsu, Japan). The total number of cells (DAPI⁺) and Ki67⁺/Sox2⁺ cells were counted in 0.3 mm² sections from three slices/mouse.

Protein determinations. Protein concentrations were determined in the cell suspensions, lysates or in parallel cell culture incubations after solubilization with 0.1 M NaOH. Protein concentrations were determined as described³⁴ using bovine serum albumin as standard.

Statistical analysis. All measurements in cell culture were carried out at least in three different culture preparations, and the results are expressed as the mean ± s.e.m. For *in vivo* experiments, we used at least four animals per condition.

For the comparisons between two groups of values, the statistical analysis of the results was performed by the Student's *t*-test. For multiple values comparisons, we used one-way analysis of variance followed by Bonferroni test. The statistical analysis was performed using the SPSS 16.0 software for Macintosh. In all cases, *P* < 0.05 was considered significant.

References

- Exner, N., Lutz, A. K., Haass, C. & Winklhofer, K. F. Mitochondrial dysfunction in Parkinson's disease: molecular mechanisms and pathophysiological consequences. *EMBO J.* **31**, 3038–3062 (2012).
- Kitada, T. *et al.* Mutations in the parkin gene cause autosomal recessive juvenile parkinsonism. *Nature* **392**, 605–608 (1998).
- Valente, E. M. *et al.* Hereditary early-onset Parkinson's disease caused by mutations in PINK1. *Science* **304**, 1158–1160 (2004).
- Beilina, A. *et al.* Mutations in PTEN-induced putative kinase 1 associated with recessive parkinsonism have differential effects on protein stability. *Proc. Natl Acad. Sci. USA* **102**, 5703–5708 (2005).
- Clark, I. E. *et al.* *Drosophila* pink1 is required for mitochondrial function and interacts genetically with parkin. *Nature* **441**, 1162–1166 (2006).
- Park, J. *et al.* Mitochondrial dysfunction in *Drosophila* PINK1 mutants is complemented by parkin. *Nature* **441**, 1157–1161 (2006).
- Corti, O. & Brice, A. Mitochondrial quality control turns out to be the principal suspect in parkin and PINK1-related autosomal recessive Parkinson's disease. *Curr. Opin. Neurobiol.* **23**, 100–108 (2013).
- Dagda, R. K. *et al.* Loss of PINK1 function promotes mitophagy through effects on oxidative stress and mitochondrial fission. *J. Biol. Chem.* **284**, 13843–13855 (2009).
- Hasson, S. A. *et al.* High-content genome-wide RNAi screens identify regulators of parkin upstream of mitophagy. *Nature* **504**, 291–295 (2013).
- McCoy, M. K. & Cookson, M. R. Mitochondrial quality control and dynamics in Parkinson's disease. *Antioxid. Redox. Signal.* **16**, 869–882 (2012).
- Gegg, M. E., Cooper, J. M., Schapira, A. H. & Taanman, J. W. Silencing of PINK1 expression affects mitochondrial DNA and oxidative phosphorylation in dopaminergic cells. *PLoS ONE* **4**, e4756 (2009).
- Morais, V. A. *et al.* Parkinson's disease mutations in PINK1 result in decreased Complex I activity and deficient synaptic function. *EMBO Mol. Med.* **1**, 99–111 (2009).
- Unoki, M. & Nakamura, Y. Growth-suppressive effects of BPOZ and EGR2, two genes involved in the PTEN signaling pathway. *Oncogene* **20**, 4457–4465 (2001).
- Lunt, S. Y. & Vander Heiden, M. G. Aerobic glycolysis: meeting the metabolic requirements of cell proliferation. *Annu. Rev. Cell Dev. Biol.* **27**, 441–464 (2011).
- Herrero-Mendez, A. *et al.* The bioenergetic and antioxidant status of neurons is controlled by continuous degradation of a key glycolytic enzyme by APC/C-Cdh1. *Nat. Cell Biol.* **11**, 747–752 (2009).
- Semenza, G. L. HIF-1 mediates metabolic responses to intratumoral hypoxia and oncogenic mutations. *J. Clin. Invest.* **123**, 3664–3671 (2013).
- Camps, C. *et al.* Integrated analysis of microRNA and mRNA expression and association with HIF binding reveals the complexity of microRNA expression regulation under hypoxia. *Mol. Cancer* **13**, 28 (2014).
- Gandhi, S. *et al.* PINK1-associated Parkinson's disease is caused by neuronal vulnerability to calcium-induced cell death. *Mol. Cell* **33**, 627–638 (2009).
- Kim, J. W., Tchernyshyov, I., Semenza, G. L. & Dang, C. V. HIF-1-mediated expression of pyruvate dehydrogenase kinase: a metabolic switch required for cellular adaptation to hypoxia. *Cell Metab.* **3**, 177–185 (2006).
- Brunelle, J. K. *et al.* Oxygen sensing requires mitochondrial ROS but not oxidative phosphorylation. *Cell Metab.* **1**, 409–414 (2005).
- Calvani, M., Comito, G., Giannoni, E. & Chiarugi, P. Time-dependent stabilization of hypoxia inducible factor-1 α by different intracellular sources of reactive oxygen species. *PLoS ONE* **7**, e38388 (2012).
- Patten, D. A. *et al.* Hypoxia-inducible factor-1 activation in nonhypoxic conditions: the essential role of mitochondrial-derived reactive oxygen species. *Mol. Biol. Cell* **21**, 3247–3257 (2010).
- Quintana-Cabrera, R. *et al.* γ -Glutamylcysteine detoxifies reactive oxygen species by acting as glutathione peroxidase-1 cofactor. *Nat. Commun.* **3**, 718 (2012).
- Priyadarshini, M., Tuimala, J., Chen, Y. C. & Panula, P. A zebrafish model of PINK1 deficiency reveals key pathway dysfunction including HIF signaling. *Neurobiol. Dis.* **54**, 127–138 (2013).
- Lin, W. *et al.* Loss of PINK1 attenuates HIF-1 α induction by preventing 4E-BP1-dependent switch in protein translation under hypoxia. *J. Neurosci.* **34**, 3079–3089 (2014).
- Scheele, C. *et al.* Altered regulation of the PINK1 locus: a link between type 2 diabetes and neurodegeneration? *FASEB J.* **21**, 3653–3665 (2007).
- Prestel, J. *et al.* Clinical and molecular characterisation of a Parkinson family with a novel PINK1 mutation. *J. Neurol.* **255**, 643–648 (2008).

28. Devine, M. J., Plun-Favreau, H. & Wood, N. W. Parkinson's disease and cancer: two wars, one front. *Nat. Rev. Cancer* **11**, 812–823 (2011).
29. Franks, P. W. *et al.* Genomic variants at the PINK1 locus are associated with transcript abundance and plasma nonesterified fatty acid concentrations in European whites. *FASEB J.* **22**, 3135–3145 (2008).
30. Tufi, R. *et al.* Enhancing nucleotide metabolism protects against mitochondrial dysfunction and neurodegeneration in a PINK1 model of Parkinson's disease. *Nat. Cell Biol.* **16**, 157–166 (2014).
31. Brix, B., Mesters, J. R., Pellerin, L. & Jöhren, O. Endothelial cell-derived nitric oxide enhances aerobic glycolysis in astrocytes via HIF-1 α -mediated target gene activation. *J. Neurosci.* **32**, 9727–9735 (2012).
32. Bolaños, J. P., Peuchen, S., Heales, S. J. R., Land, J. M. & Clark, J. B. Nitric oxide-mediated inhibition of the mitochondrial respiratory chain in cultured astrocytes. *J. Neurochem.* **63**, 910–916 (1994).
33. Paxton, R. & Sievert, L. M. An improved assay for pyruvate dehydrogenase in liver and heart. *Biochem. J.* **277**, 547–551 (1991).
34. Lowry, O. H., Rosebrough, N. J., Lewis-Farr, A. & Randall, R. J. Protein measurement with the Folin phenol reagent. *J. Biol. Chem.* **193**, 265–275 (1951).

Acknowledgements

This work was funded by the Spanish Ministerio de Economía y Competitividad (to J.P.B., grant number SAF2013-41177-R), the Instituto de Salud Carlos III (to J.P.B., grant number RD12/0043/0021; to A.A., grant numbers PI12/00685 and RD12/0014/0007), Junta de Castilla y León (to J.P.B., SA003U13), the SP3-People-MC-ITN programme of

the European Commission (to J.P.B., 608381 TINTIN), and the European Regional Development Fund. I.L.-F. is the recipient of a FPI Fellowship from the MINECO (Spain). The technical assistances of Ms. Monica Carabias, Ms. Monica Resch, Dr Nicoleta Moisoi, Dr Kate Dudek and Dr Jin Li Luo are acknowledged.

Author contributions

J.P.B. conceived the idea. L.M.M. provided conceptual advice and contributed materials. J.P.B., R.R.-A., E.F. and A.A. designed research. R.R.A., I.L.-F., E.F., A.A. and L.M.M. performed research. J.P.B., R.R.A., A.A., E.F. and L.M.M. analysed the data. J.P.B. wrote the manuscript.

Additional information

Accession codes: Microarray raw data are available in the ArrayExpress database (www.ebi.ac.uk/arrayexpress) under the accession number E-MTAB-2462.

Supplementary Information accompanies this paper at <http://www.nature.com/naturecommunications>

Competing financial interests: The authors declare no competing financial interests.

Reprints and permission information is available online at <http://npg.nature.com/reprintsandpermissions/>

How to cite this article: Requejo-Aguilar, R. *et al.* PINK1 deficiency sustains cell proliferation by reprogramming glucose metabolism through HIF1. *Nat. Commun.* 5:4514 doi: 10.1038/ncomms5514 (2014).